Energy Materials

Supplementary Materials

Enhanced photodegradation of ciprofloxacin with organic photocatalyst through a ternary strategy

Yang Zhou[1,#], Ciyuan Huang[1,#], Linji Yang[1,#], Ruirui Zhang[1,2], Yanzhen Yin[2,*], Cong Liu[1], Ke Sun[3], Shangfei Yao[1], Nannan Geng[1], Yu Luo[5], Tao Yang[4], Bingsuo Zou[1], Tao Liu[1,3,*]

[1]School of Chemistry and Chemical Engineering, State Key Laboratory of Featured Metal Materials and Life-cycle Safety for Composite Structures, School of Resources, Environment and Materials, Guangxi University, Nanning 530004, Guangxi, China.

[2]Guangxi Key Laboratory of Green Chemical Materials and Safety Technology, Beibu Gulf University, Qinzhou 535000, Guangxi, China.

[3]Department of Biochemistry and Cell Biology, Youjiang Medical University for Nationalities, Baise City 533000, Guangxi, China.

[4]Centre for Mechanical Technology and Automation, Department of Mechanical Engineering, University of Aveiro, 3810-193 Aveiro, Portugal.

[5]Kennedy Krieger Institute, Johns Hopkins University, Baltimore, MD 21205, USA.

[#]Authors contributed equally.

Correspondence to: Prof. Yanzhen Yin, Guangxi Key Laboratory of Green Chemical Materials and Safety Technology, Beibu Gulf University, 12 Binhai Avenue, Binhai New City, Qinzhou 535000, Guangxi, China. E-mail: Yinyinyanzhen2009@163.com; Prof. Tao Liu, School of Chemistry and Chemical Engineering, State Key Laboratory of Featured Metal Materials and Life-cycle Safety for Composite Structures, School of Resources, Environment and Materials, Guangxi University, No.100, Daxue East Road, Nanning 530004, Guangxi, China. E-mail: liutaozhx@gxu.edu.cn

Materials

PM6 (Poly[[4,8-bis[5-(2-ethylhexyl)-4-fluoro-2-thienyl]benzo[1,2-b:4,5-b′]dithiophene-2,6-diyl]-2,5-thiophenediyl[5,7-bis(2-ethylhexyl)-4,8-dioxo-4H,8H-benzo[1,2-c:4,5-c′]dithiophene-1,3-diyl]-2,5-thiophenediyl]).

Y6 (2-[2-[[23-[[1-(dicyanomethylidene)-5,6-difluoro-3-oxoinden-2-ylidene]methyl]-3,27-bis(2-ethylhexyl)-

8,22-di(undecyl)-6,10,15,20,24-pentathia-3,14,16,27-tetrazaoctacyclo[16.9.0.02,12.04,11.05,9.013,17.019,26.021,25]heptacosa-1(18),2(12),4(11),5(9),7,13,16,19(26),21(25),22-decaen-7-yl]methylidene]-5,6-difluoro-3-oxoinden-1-ylidene]propanedinitrile).

ITCPTC (3,9-bis(2-methylene-(3-(1,1-dicyanomethylene)-cyclopentane-1,3-dione-[c]thiophen))-5,5,11,11-tetrakis(4-hexylphenyl)-dithieno[2,3-d:2′,3′-d′]-s-indaceno[1,2-b:5,6-b′]dithiophene).

Characterization

The morphology images of photocatalysts were obtained from scanning electron microscope (SEM, Zeiss Sigma 300), and elemental mapping was achieved during SEM by energy-dispersive X-ray spectroscopy (EDS). The UV–vis diffuse reflectance spectra were obtained by SHIMADZU UV-2600i＆ISR-2600Plus. Photoluminescence (PL) spectra were taken on an Edinburgh Instrument FLS 1000. The Brunauer-Emmett-Teller (BET) calculation was used to investigate the specific surface area (ASAP 2460 3.01 analyzer). The electron spin resonance (ESR) investigations were operated on an ESR spectrometer (ESR, Bruker EMXplus).

Photoelectrochemical measurements of materials were measured using an electrochemical workstation (CHI-660 E, Chenhua, China) with a general three-electrode configuration. Ag/AgCl electrode as the reference electrode, Pt as the counter electrode, the photocatalysts served as the working electrode, and Na_2SO_4 solution (0.5 M) as the electrolyte. Electrochemical impedance spectroscopy (EIS) was performed over the frequency range of 10^5 Hz to 0.1 Hz. Transient photo-current response test were carried out with an Xe lamp as the light source. The J-V curves were obtained using the SS-F5-3A solar simulator (Enli Technology CO, Ltd.) under AM 1.5G light source.

Active species trapping experiments

1.0 mM 1,4-benzoquinone (t-BQ), 1.0 mM EDTA-2Na, 1.0 mM IPA were applied for superoxide radical ($\cdot O_2^-$), hole (h^+) and hydroxyl radical (·OH), respectively. Moreover, ESR experiment used 5,5-Dimethyl-1-pyrroline N-oxide (DMPO) as scavengers to determine ·OH, $\cdot O_2^-$radicals and used 2,2,6,6-Tetramethylpiperidine-1-oxyl (TEMPO) as scavengers to determine h^+.

Table 1. SEM-EDS element proportion of (A) CSC-PM6: Y6: ITCPTC and (B) CSC-TiO_2

(A)

Element	Line type	Wt%
C	K-line system	41.20
N	K-line system	2.37
O	K-line system	47.53
F	K-line system	1.25
S	K-line system	7.65

(B)

Element	Line type	Wt%
C	K-line system	66.78
Ti	K-line system	33.22

Table 2. BET specific surface area and pore diameter of the as-prepared samples

Samples	S_{BET} (m^2/g)	Pore diameter (nm)
CSC	932.5200	2.0754
CSC-PM6: Y6: ITCPTC	894.1811	2.0895

Table 3. OPV device performance of Y6: ITCPTC

Samples	V_{OC} (V)	J_{SC} (mA/cm2)	FF (%)	PCE (%)
1:0	0.593	0.362	0.316	0.068
0.5:0.5	0.739	0.384	0.298	0.084
0:1	0.840	0.506	0.228	0.097

Table 4. Hole and Electron mobility of PM6: Y6: ITCPTC

Samples	Hole mobility	Electron mobility
1:1:0	0.000591	0.000331
1:0.5:0.5	0.000646	0.000445
1:0:1	0.000581	0.000311

Table 5. Detailed information of adsorption capacity and isotherm

Type	Model	Equation	Parameters
Adsorption capacity		$q_t = \frac{(C_0 - C_t)V}{m}$	V (L): reaction solution volume, m (g): the mass of the adsorbent.
Kinetics model	pseudo-first-order	$\log(q_e - q_t) = \log q_e - \frac{k_1}{2.303}t$	q_e (mg/g): equilibrium adsorption capacity, q_t (mg/g): the sorption amount at time t, k_1 (1/min): the adsorption rate constant.
	pseudo-second-order	$\frac{t}{q_t} = \frac{t}{q_e} + \frac{1}{k_2 q_e^2}$	k_2 (g/mg·min) : the rate constant determined by the plots of t/q_t versus t.
Isotherm model	Langmuir	$\frac{C_e}{q_e} = \frac{1}{q_m K_L} + \frac{C_e}{q_m}$ $R_L = \frac{1}{1 + K_L C_e}$	q_e (mg/g): equilibrium adsorption capacity, C_e (mg/L): solution equilibrium concentration, q_m (mg/g): maximum adsorption capacity, K_L (L/mg): Langmuir constant, R_L: the separation factor.
	Freundlich	$\ln q_e = \frac{1}{n}\ln C_e + \ln K_F$ $K_F = \frac{Q_m}{C_H^{1/n}}$	K_F (L/mg) and n: the Freundlich constants, which represent the adsorption capacity and intensity, C_H (mg/L): the initial CIP concentration

Table 6. Detailed information of Kinetic parameters for CIP adsorption

Samples	Pseudo-first-order model			Pseudo-second-order model	
	$q_{e,exp}$ (mg/g)	$q_{e,cal}$ (mg/g)	R^2	$q_{e,cal}$ (mg/g)	R^2
CSC-PM6: Y6: ITCPTC	259.2	270.145	0.9956	336.160	0.9866
CSC	219.2	227.851	0.9970	284.531	0.9902

Table 7. Summary of photodegradation of CIP reported in recent years

Photocatalyst	Concentration (mg/L)	Time (min)	Efficiency (%)	Reference
Bi/Bi_2O_3/TNAs	10	300	90.3	[1]
ZIF-8-derived CuS/ZnO	10	40	94.59	[2]

WSe_2 NPs	10	100	93.4	[3]
TiO_2/ Bi_2MoO_6/Ag	10	100	83.58	[4]
$BiOCl/BiOIO_3$	15	60	88	[5]
$BiBDC/BiVO_4$	10	60	76.3	[6]
CSC-PM6: Y6: ITCPTC	10	45	97.3	This work

Table 8. The activation energy of different reaction pathways

Pathway	**Reaction process**	**E_a (kJ/mol)**
I	CIP→P1	612.356
II	CIP→P5	197.012
III	CIP→P7	536.085

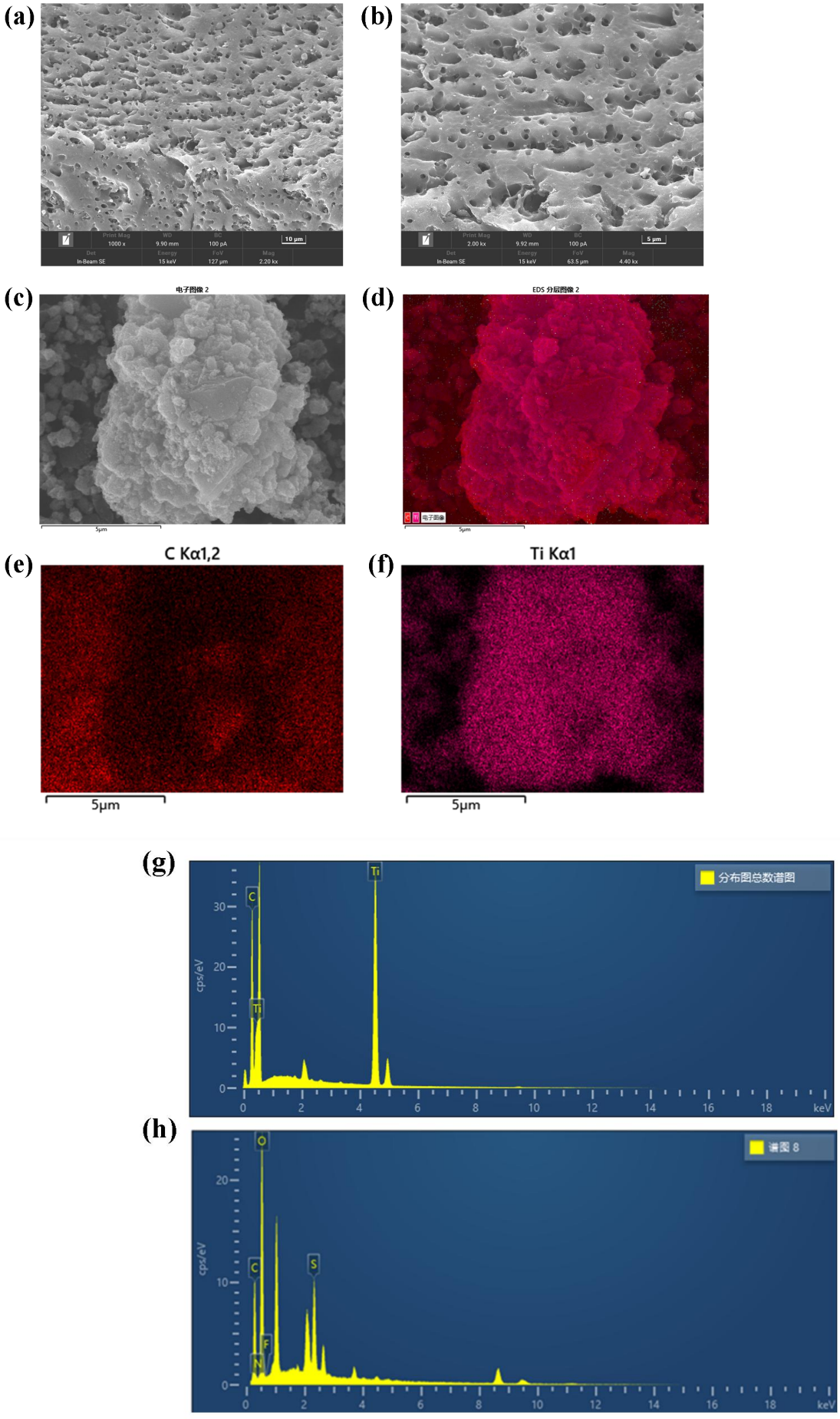

Figure 1. SEM images of CSC-PM6: Y6: ITCPTC (a, b), SEM-EDS images of CSC-TiO_2 (c, d, e, f, g), and EDS images of CSC-PM6: Y6: ITCPTC (h).

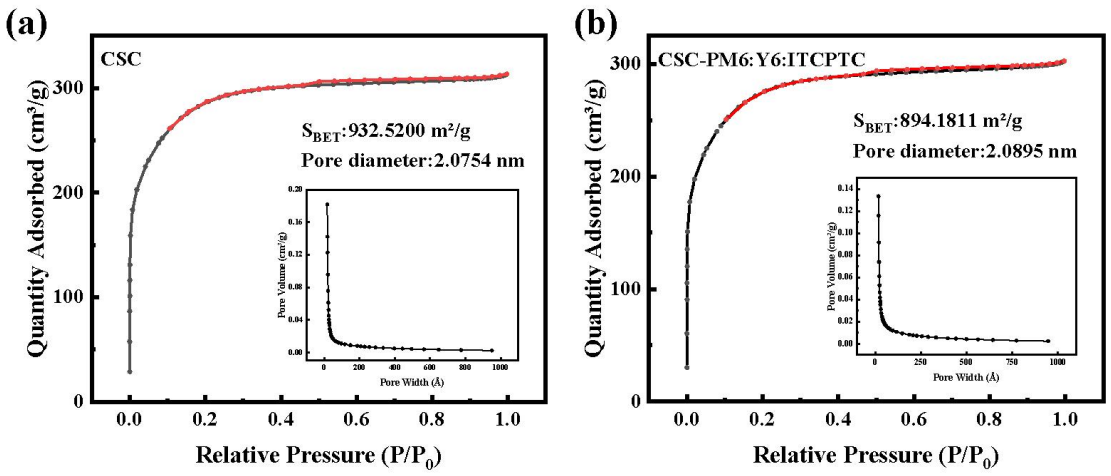

Figure 2. The N_2 adsorption–desorption isotherms and pore size distribution curves of (a) CSC and(b) CSC-PM6: Y6: ITCPTC.

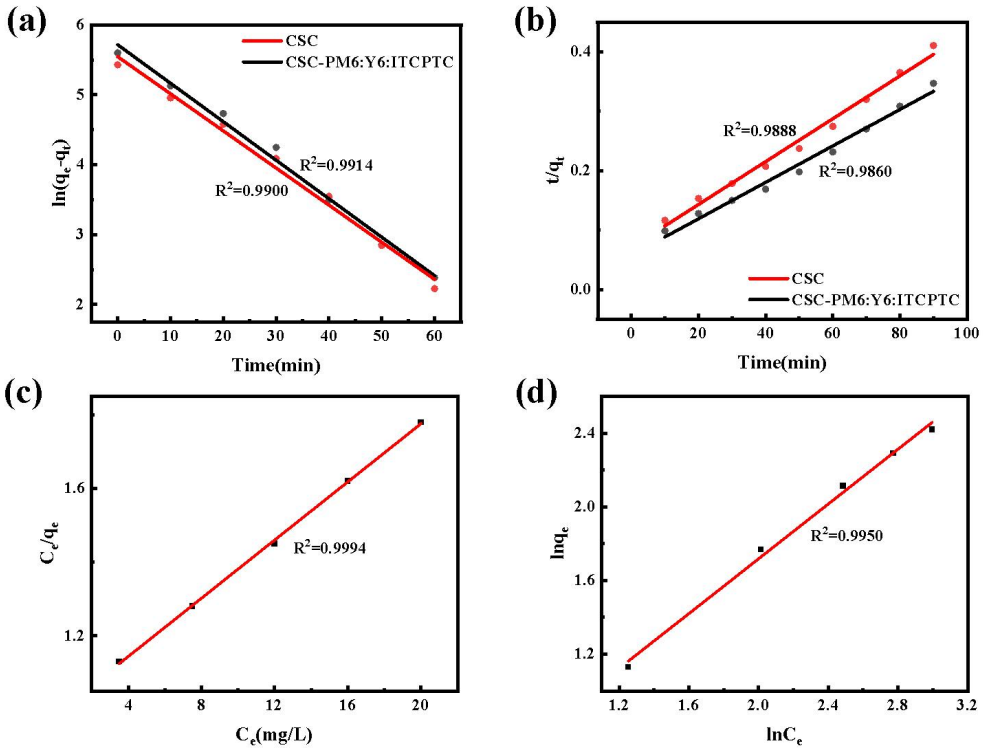

Figure 3. Effect of contact time on the adsorption of CIP to the samples under dark conditions, the pseudo-first-order model (a) and the pseudo-second-order model (b) of samples, the Langmuir model (c) and the Freundlich model (d) for CIP adsorption.

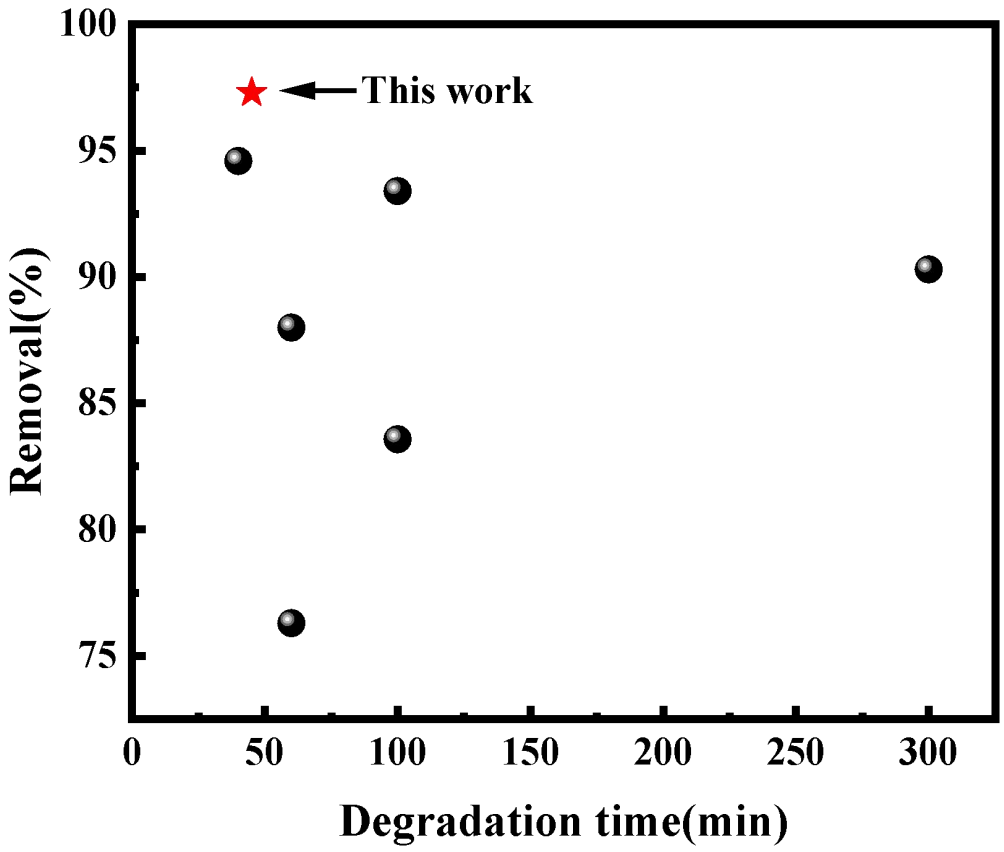

Figure 4. Comparison of degradation performance of CIP by different photocatalysts.

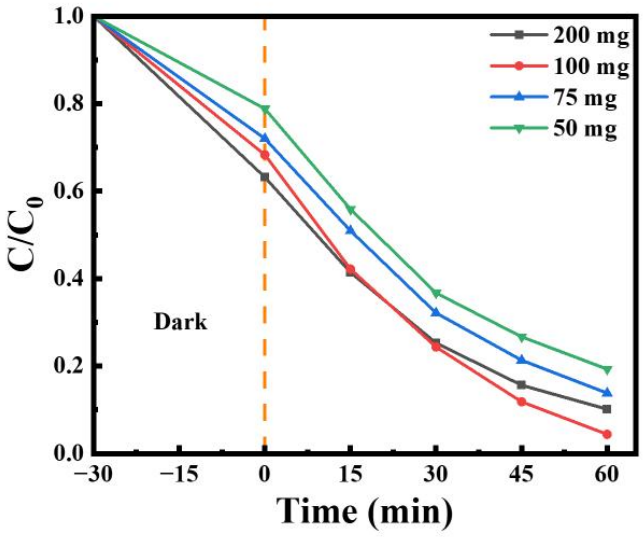

Figure 5. Photodegradation of CIP under different catalyst dosages.

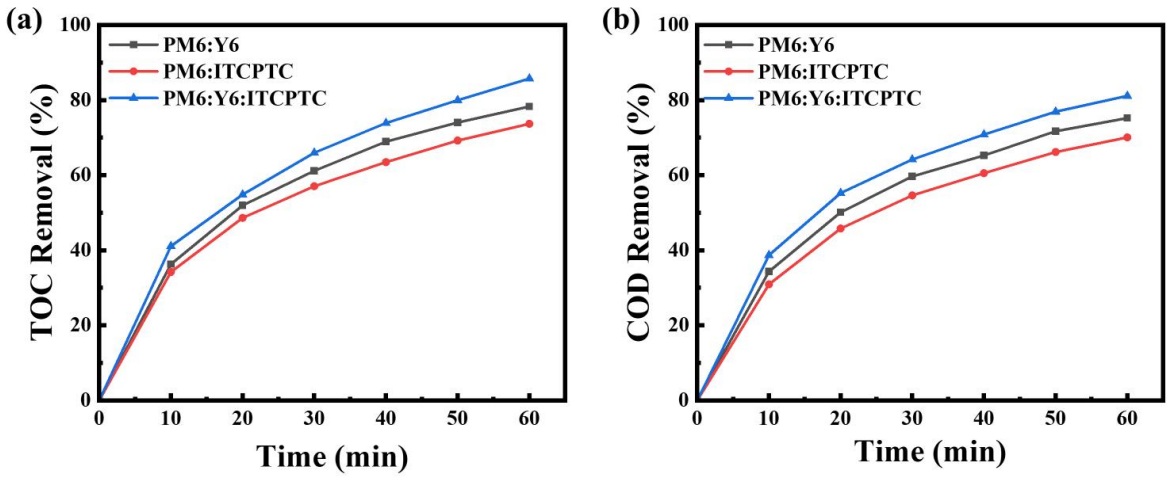

Figure 6. (a) TOC and (b) COD removal (%) for CIP degradation.

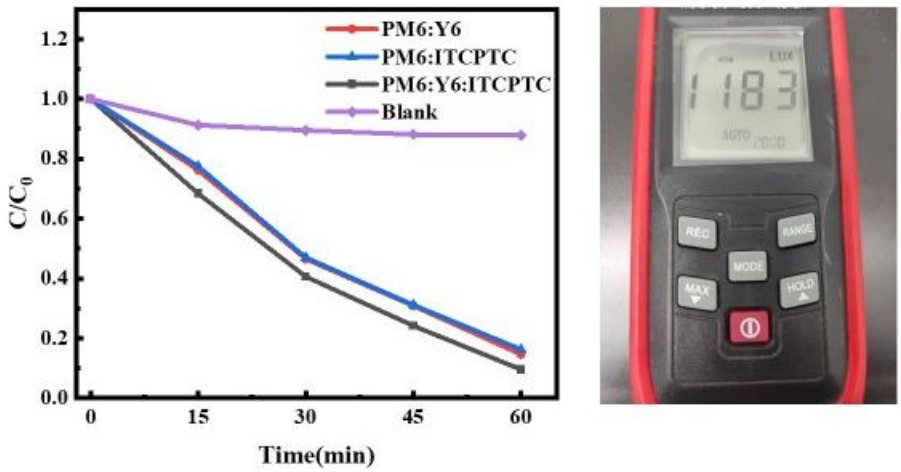

Figure 7. Photocatalytic degradation of CIP under indoor light irradiation.

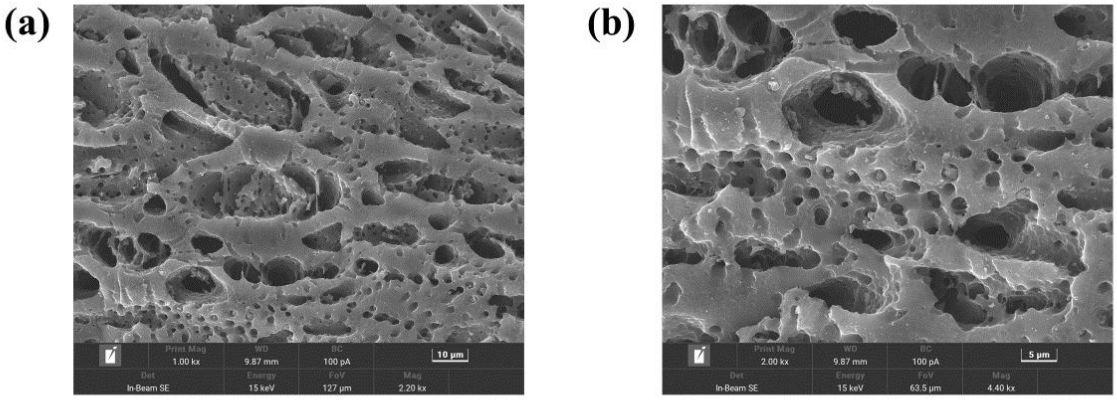

Figure 8. (a, b) SEM image of catalyst after degradation.

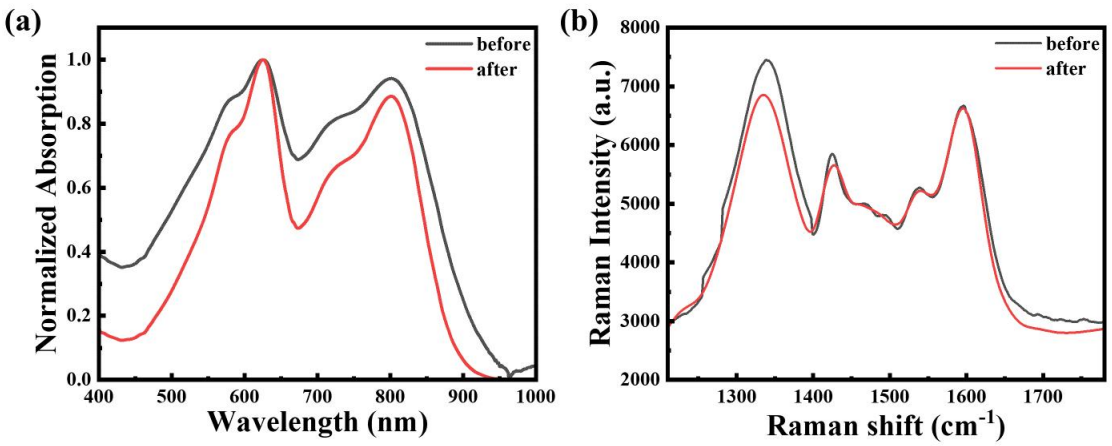

Figure 9. (a) UV-vis absorption and (b) Raman spectrum of catalyst before and after degradation.

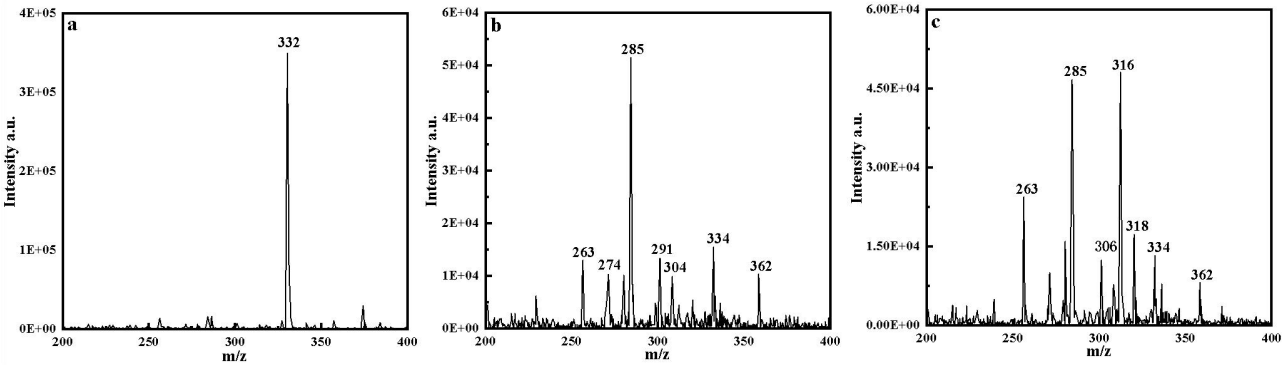

Figure 10. The mass spectrum of the intermediates of CIP.

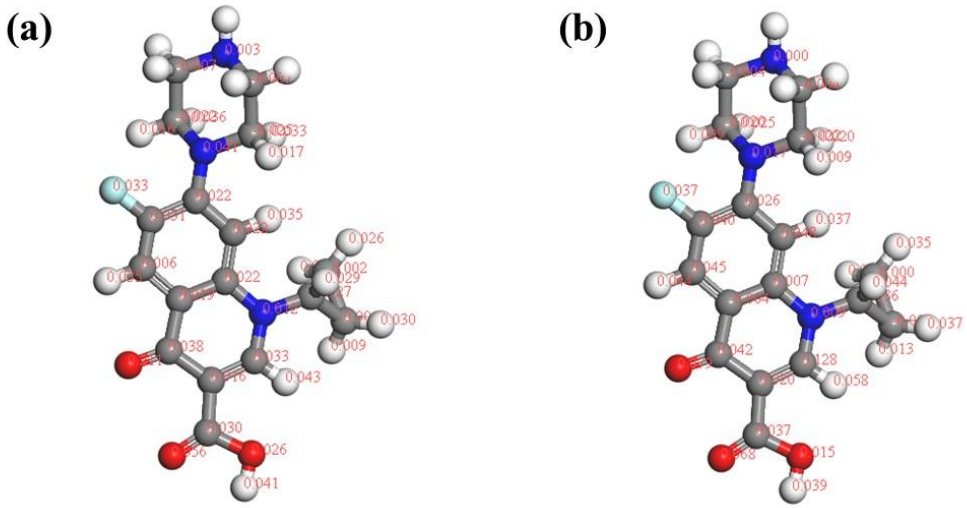

Figure 11. The Fukui value results of CIP, (a) f^- and (b) f^+.

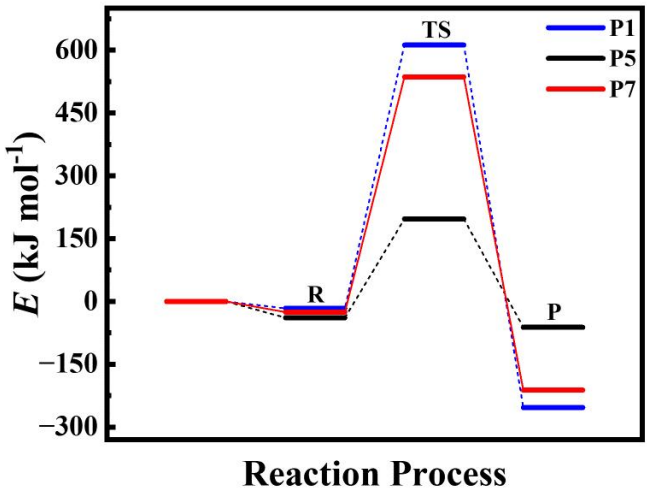

Figure 12. Gibbs free energy of different reaction pathways.

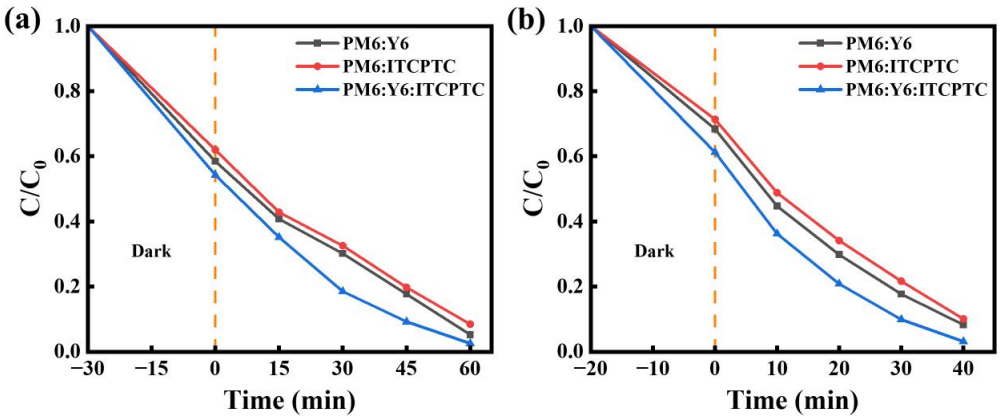

Figure 13. Photodegradation of (a) NOR (10 mg/L) and (b) TC (10 mg/L) under Xe lamp.

REFERENCES

[1] B. Yan, G. Chen, B. Ma, Y. Guo, Y. Zha, J. Li, S. Wang, J. Liu, B. Zhao, H. Xie, Construction of surface plasmonic Bi nanoparticles and α-Bi2O3 co-modified TiO2 nanotube arrays for enhanced photocatalytic degradation of ciprofloxacin: Performance, DFT calculation and mechanism, Separation and Purification Technology, 330 (2024) 125180.

[2] A. Mariappan, P. Mannu, T. Thiruppathiraja, T.T.T. Nga, S. Lakshmipathi, C.-L. Dong, R.K. Dharman, T.H. Oh, Interfacial oxygen vacancy modulated ZIF-8-derived ZnO/CuS for the photocatalytic degradation of antibiotic and organic pollutants: DFT calculation and degradation pathways, Chemical Engineering Journal, 476 (2023) 146720.

[3] L. Chen, Y. Chuang, T.-B. Nguyen, C.-H. Wu, C.-W. Chen, C.-D. Dong, A novel tungsten diselenide nanoparticles for enhanced photocatalytic performance of Cr (VI) reduction and ciprofloxacin (CIP), Chemosphere, 339 (2023) 139701.

[4] J. Tong, H. Zhai, S. Zhao, L. Song, G. Wang, N. Feng, P. Tan, J. Xie, J. Pan, Visible light-driven sliver-modified titanium dioxide / bismuth molybdenum oxide with rapid interfacial charge-transfer for dual highly efficient photocatalytic degradation and disinfection, Journal of Colloid and Interface Science, 653 (2024) 285-295.

[5] Z. Guo, Y. Cheng, X. Chang, J. Liu, Q. Feng, Q. Yan, Internal electric field and oxygen defect synergistically optimized of BiOCl/BiOIO3 heterojunctions for enhancing charge transfer: Insight into a nature-derived method for Fermi level modulation, Chemical Engineering Journal, 474 (2023) 145575.

[6] B. Zhang, H. Xu, M. Wang, L. Su, C. Wu, Q. Wang, Construction of a novel Bi-MOF/BiVO4 heterojunction with enhanced visible light photocatalytic performance, Journal of Environmental Chemical Engineering, 11 (2023) 110417.